



# Isometric Torque Values About Robotic Knee Using Braided Pneumatic Actuators

Ben Bolen<sup>1,\*</sup>, Lindie Burgess<sup>1</sup>, Connor Morrow<sup>1</sup>, Aidan Vogt<sup>1</sup>, Cody Scharzenberger<sup>1</sup>, Lawrence Pang<sup>1</sup>, and Alex Hunt<sup>1</sup>

<sup>1</sup>*Agile and Adaptive Robotics Laboratory, Portland State University, Department of Mechanical and Materials Engineering, Portland, OR, USA*

Correspondence\*:

Ben Bolen, Portland State University, Department of Mechanical and Materials Engineering, 1930 SW 4th Ave., Portland, OR, 97207, USA  
bbolen83@gmail.com

## ABSTRACT

A lower limb model of a bipedal humanoid robot was designed to achieve biomimetic ranges of motion and isometric torque values. An important component of this robot is a biomimetic four-bar linkage knee joint that allows the joint to have two degrees of freedom (DoF) over a range of knee flexion and extension values. This joint is actuated with artificial muscles called braided pneumatic actuators (BPAs). While these artificial muscles have force-length curves that are grossly similar to real muscles, they have other limitations that need to be considered, such as their lower maximum contractile capacity and flexibility when compared to human muscles. An isometric robot knee torque test stand was created to determine several things. The first task was to quantify results for actuators of different initial length and configuration. Second, use that data to characterize the difference between theoretical calculations and actual results so that we may modify the theoretical calculations. To do this, we simplified the muscle arrangement on the robotic leg so that it consists of a pair of antagonistic uniarticular flexor/extensor muscles. Another robot knee was designed using similar muscle origin insertion locations but this knee was used a simpler 1-DoF revolute joint. Testing for isometric knee torque values in these configurations allowed for the quantification of difference between measured and expected results, as well as a quantification of the factors that were important in these differences.

**Keywords:** BPA, Biomimetic, Function Fit, PAM, Artificial Muscle, Bioinspired, Bipedal Robot, Isometric Knee Torque

## 1 INTRODUCTION

Both academic researchers and the general public are keenly interested in biomimetic humanoid robots due to their many applications. In the discipline of biomimetic robotics, high fidelity humanoid robots can help improve our understanding of both human biomechanics and the underlying neuromechanical systems that control them (Shin et al., 2018; Asano et al., 2019). Experiments can be done with robots that would not be practical nor ethical if done on human test subjects, and modifying robotic platforms is a potentially faster and cheaper alternative to human observation studies.

For truly biomimetic humanoid robots to go a step beyond being merely bio-inspired, it is unclear how the actuator affects other aspects of the control. One requirement for proposed artificial muscle-actuators should be that they be able to produce isometric torque about humanoid joints that meets or exceeds values

measured in humans. There are several interesting methods of actuating robotic joints, including artificial muscles, electric motors (either directly driving the joints (citations?) or via cable systems (citations?)), or hydraulics. Electric motors tend to require a lot of power, generate a lot of heat, and have torque curves unlike that of real muscles. Hydraulic actuators are heavy and require a dedicated hydraulic fluid system to operate. Electrically stimulated artificial muscles are new and do not yet produce very much force. McKibben style braided pneumatic actuators (BPAs, also called Pneumatic Artificial Muscles or PAMs) are a promising method of actuation because they have low weight, high force/weight ratio, and a force-length curve that is grossly similar to actual muscle. Routing these muscles in a biomimetic arrangement can allow us to investigate and mimic the torque produced about joints by actual human muscle.

Previous robots that use artificial muscles do not show significant design considerations for the forces and torques that the muscles will produce. However, these aspects are critical for further understanding how muscles are controlled (citation?) in animals. As a consequence of this, these robots typically do not faithfully attempt to replicate the number of existing muscle actuators. They also tend to use a single degree of freedom (DoF) knee joints, while knees are actually better modeled as 2-DoF sliding and rotating joints. They instead focus on planar, uniarticular muscle arrangements. Our research diverges from these robots by attempting to correct for these deficiencies.

Our previous research has laid the groundwork to start building a bipedal robot with biomimetic humanoid joints and artificial muscle actuator paths. Investigating the isometric force profile of 10 mm Festo Braided Pneumatic Actuators (BPAs, also called Pneumatic Artificial Muscle or PAMs) demonstrated artificial muscles that can be made to have a similar isometric force profile to human muscle (Hunt et al., 2017). Research on a humanoid artificial knee allowed us to build a biomimetic translating sliding knee joint (Steele et al., 2017) instead of the traditional pinned robotic joint. A more recent paper on artificial muscle attachment locations for a humanoid robot produced theoretical isometric torque curves (Bolen and Hunt, 2019). Optimization of these muscle paths and attachment locations was done by Morrow to produce a torque curve and muscle path that match the robotic system more closely to the human biomechanical benchmark we are using (Morrow et al., 2020). All of the concepts can be combined to build an artificial human leg and test the validity of our theory.

These previous studies need to be combined and tested on a physical robot body. The 10 mm Festo BPAs have been characterized (Hunt et al., 2017), but the 20 mm and 40 mm BPAs have not been. In our previous work (Bolen and Hunt, 2019; Morrow et al., 2020), moment arms have been calculated by the unit vector cross product method presented show in Hoy (Hoy et al., 1990), but not the change in muscle length over change in angle method that Hoy and others (Hoy et al., 1990; Yamaguchi and Zajac, 1989; Sherman et al., 2013; Delp et al., 1990; Seth et al., 2011) have also used. It is not known if one method is more correct than the other. Knee Instantaneous Center of Rotation (ICR) differs between the Steele model (Steele et al., 2018) and the OpenSim model Delp et al. (1990); Seth et al. (2018) model. This fact, as well as changes in the knee geometry and muscle placement, means there will be different muscle moment arms between the models. The differences in isometric torque between the theoretical, measured, and human biomechanical benchmark model need to be investigated.

Deviation from expected versus measured force in BPAs can happen in several ways. Festo reports that there can be a 10% deviation from theoretical force ((Corporation, 2022)). Joint friction can cause a decrease in torque, as can non-rigid elements of the artificial leg and test frame. Kinking of the artificial muscle as it wraps around a joint also is predicted to reduce the amount of available force. A further reduction in force, and therefore torque, can be expected from a previously undefined reduction in force that happens as BPAs resting length is decreased.

We hypothesize that the isometric torque values that we measure experimentally will be lower than what is predicted by our theoretical model. A correction factor can then be applied to our calculations which will improve our results. The modified design tools we previously developed can be compared to measured isometric torque values produced by our artificial muscles about the robot knee joint, which will then be used to update how we design and analyze biomimetic joints in the future (including determining which, if any, method of calculating moment arm is the best). Future designs can then be built with artificial muscles that meet or exceed human isometric torque values.

## 2 METHODS AND MATERIALS

An important initial step for biomimetic humanoid robot research is to see if these robots, actuated by artificial muscles, can meet or exceed isometric torque values that are produced by human muscles (or groups of muscle actuators, in some cases). Previous research has demonstrated meeting or exceeding these human values with BPAs is at least theoretically plausible (Bolen and Hunt, 2019; Morrow et al., 2020), so the next logical step is to test this on an actual robot. To accomplish this, we built a test jig to run these experiments. With the expectation that measured results will be less than theoretical, it was also necessary to simplify the robot muscle arrangement and knee design to elucidate the variables that affect the results. There are, therefore, three models that we must consider, including: (1) the human biomechanical model, (2) the conceptual robot model, and (3) the actual robot model. Within the conceptual and actual robot models, we varied the knee actuation by using either a simplified pinned knee joint or a biomimetic 2-DoF knee, and muscles to either flex or extend the joint. Furthermore we varied the artificial muscle origin/insertion locations, resting lengths, diameters, and whether or not they used an artificial tendon. These results were compared to the baseline model.

After running these tests it was important to verify that the equation developed in (Hunt et al., 2017) was applicable to longer resting BPA lengths and forces in (Bolen and Hunt, 2019; Morrow et al., 2020). Comparing the discrepancy in force values expected from this equation to values we determined experimentally with additional BPA lengths, it was necessary to derive additional equations to characterize the Festo BPAs. During this process, we found an equation for maximum force in the 10 mm BPA as a function of resting length, a normalized equation for force as a function of relative strain and relative pressure, and were unable to find a relationship between maximum contraction and resting length.

### 2.1 Robot Architecture

The biomimetic robot leg assembly is for a two legged robot with 2-DoF knee joint first introduced in (Steele et al., 2017). The 2-DoFs are achieved by using a four bar linkage mechanism. The leg assembly is based off of bones scans of someone 6 ft tall (approx. 1.83 m) and the OpenSim Gait2392 model. Each joint is driven by two antagonistic Festo actuators which act as artificial muscles. A test jig constrains the robot to sagittal planar motion. This system has two mounting locations to fix the femur to the frame. To eliminate the effect of gravity on our test results the robot sagittal plane was made parallel with the horizontal plane of the ground. This enables longitudinal, vertical, and pitch movements (e.g. knee joint flexion/extension), while constraining lateral, roll, and yaw DoFs.

The actuators are Festo brand BPAs of internal diameter (ID) 10 mm, 20 mm and 40 mm size. Each actuator is connected in series with a Freescale MPX5700 GP gauge pressure sensor. Joint and load cell angles are collected with digital or analog goniometers. Analog data from the pressure sensor is converted to digital data with a microcontroller, which then passes that data on to a Windows 10 PC or a Windows 11 laptop. Force is measured by reading the screen of a crane scale or using a load cell. When using a load

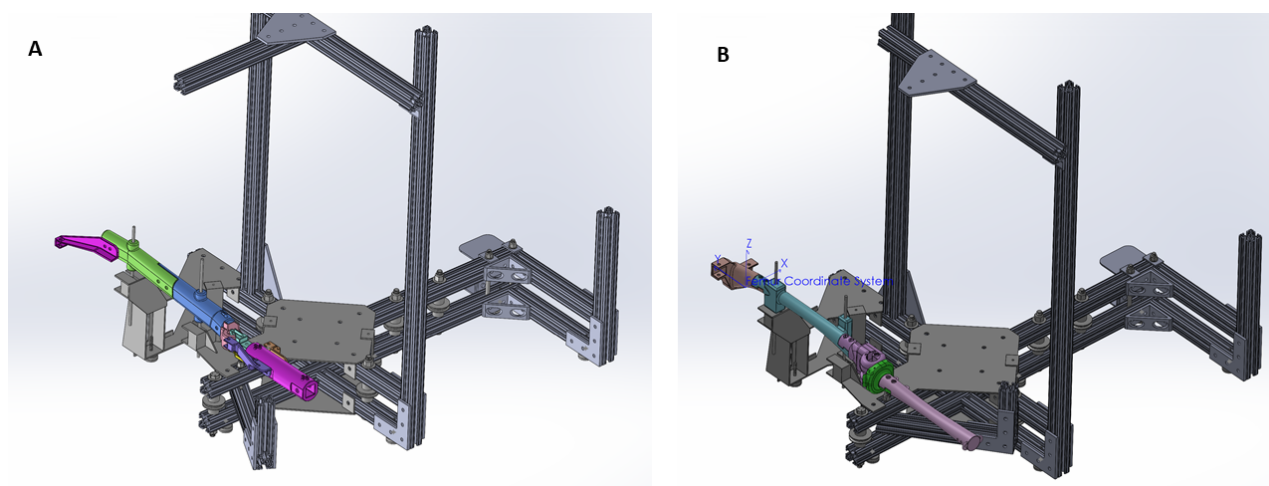


**Figure 1.** Solid model assemblies of two different robotic legs in the test stand using either (A) a revolute joint knee, or (B) a biomimetic knee.

cell the data is passed to a HX711 24-bit analog-to-digital converter (ADC), and then the microcontroller to computer connection previously mentioned.

Components of the robot leg are the knee joint, femur, tibia, BPAs, BPA end caps, artificial tendon (where noted), and attachment brackets 2. The artificial bone components are 3D printed using Onyx material on Markforged Onyx One and Mark Two printers. Onyx is a proprietary Markforged material that consists of chopped carbon fiber in nylon. Certain brackets also included carbon fiber layers to increase stiffness. Artificial tendon is made with Shimano bicycle brake cable for 10 mm diameter BPA, and wire rope with the larger diameter BPAs. When using the brake cable we first apply load to it and induce plastic deformation so that during the test the cable only has elastic deformation.

In many cases, the goal is to determine the maximum isometric torque a BPA can produce in a given configuration. Therefore the BPAs must be inflated full pressure (which we defined as the somewhat standard building air supply pressure of 620 kPa). We chose to use one uniarticular knee extensor and one uniarticular knee flexor. The revolute joint knee tests used 10 mm Festo BPAs only. The Biceps Femoris Short Head muscle was mimicked using a 20 mm Festo BPA. The human vastus intermedius, vastus lateralis, and vastus medialis are mimicked using one over-strength robotic vastus intermedius BPA of 40 mm internal diameter (ID). We designed our own end caps for the actuators and printed them in Onyx. One of the cap styles is designed to be pinned to the muscle origin location, while the other style of end cap style is free floating and attaches to the muscle insertion location via an artificial tendon. During tests where both ends were pinned, only the former style of end cap was used.

Larger diameter BPA lengths for the humanoid knee were determined using the optimization procedure described by (Morrow et al., 2020). Actuator origin and insertion attachment points locations are in the femoral and tibial reference frames. These reference frames are discussed in the next section.

### 2.1.1 Robotic Knee Joints

We used the sliding contact knee that was designed by Steele (Steele et al., 2018, 2017). The knee is sliding contact and was designed to reduce wear. In practice, not much contact occurred between the condylar surface and the tibial head. This design uses a four bar linkage that allows the joint origin to translate in the  $\hat{y}$  and  $\hat{z}$  directions during knee rotation. Typically, a reference is located at the joint center.

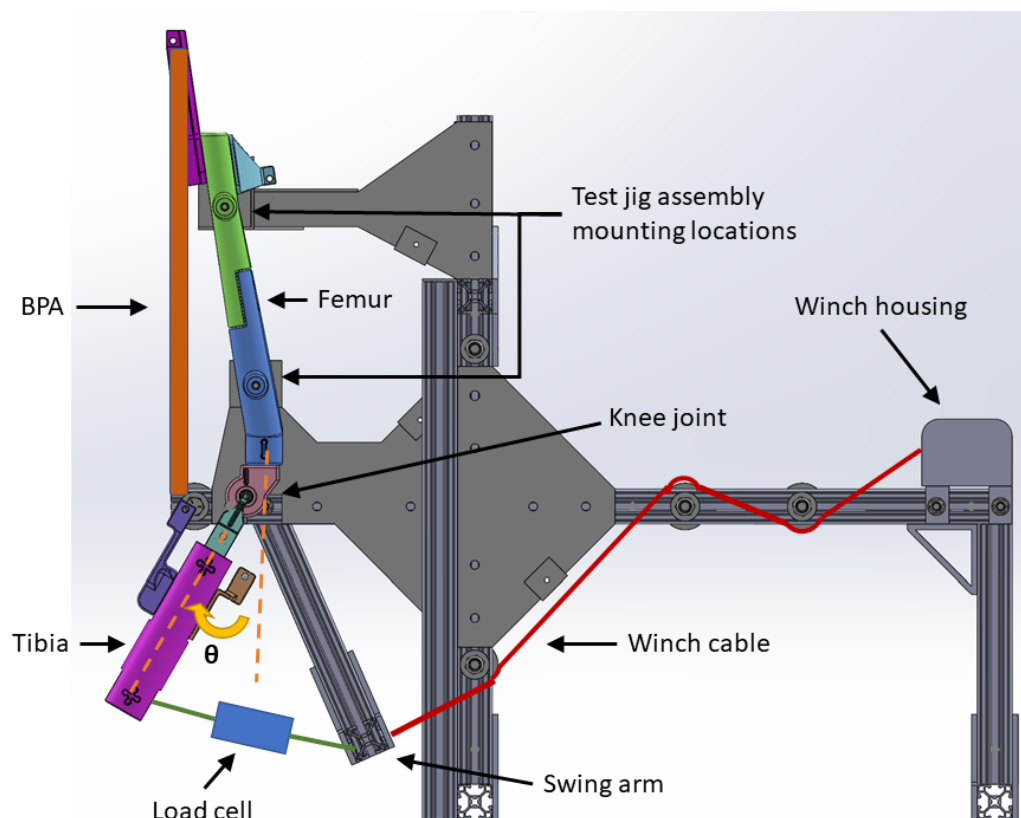


**Figure 2.** 1-DoF pinned-joint robot knee in the test apparatus with important components labeled. Leg is shown with 30 degrees flexion, i.e.  $\theta_k = -30^\circ$

141 The linkage has an Instantaneous Center of Rotation (ICR) at the intersection of the links. To more directly  
 142 compare our results with the OpenSim model, and in the interest of simplifying our model's transformation  
 143 matrices, we arbitrarily defined a joint location that moved in a similar way to the human biomechanical  
 144 model 3. Both models had the same home position location, as did the pinned knee joint.

145 The differences in the knee X and Y position as a function of knee angle are show in ???. The muscle  
 146 origin and insertion locations for each configuration is listed in 1. With the reference frames and muscle  
 147 path geometry defined, it is then possible to calculate torque values that the muscles can produce about the  
 148 joint.

## 149 2.2 Moment arm and Torque calculations

150 Compare measured robot performance to robot calculations, but also to what we expected from a human's  
 151 reported maximum isometric force. Given a point of interest and a force vector  $\vec{F}$ , there exists a distance  $\vec{d}$   
 152 from the point of interest to the line of action represented by  $\vec{F}$ . The classical mechanics way to calculate  
 153 torque  $\vec{M}$  about the point of interest is to take the cross product of distance  $\vec{d}$  and force vector  $\vec{F}$  1.

$$\vec{M} = \vec{d} \times \vec{F} \quad (1)$$

154 The calculations for human muscle force that we used as a benchmark were from Delp, Hoy, Yamaguchi,  
 155 Sherman, Millard, and Thelen (Delp et al., 1990; Hoy et al., 1990; Yamaguchi and Zajac, 1989; Sherman



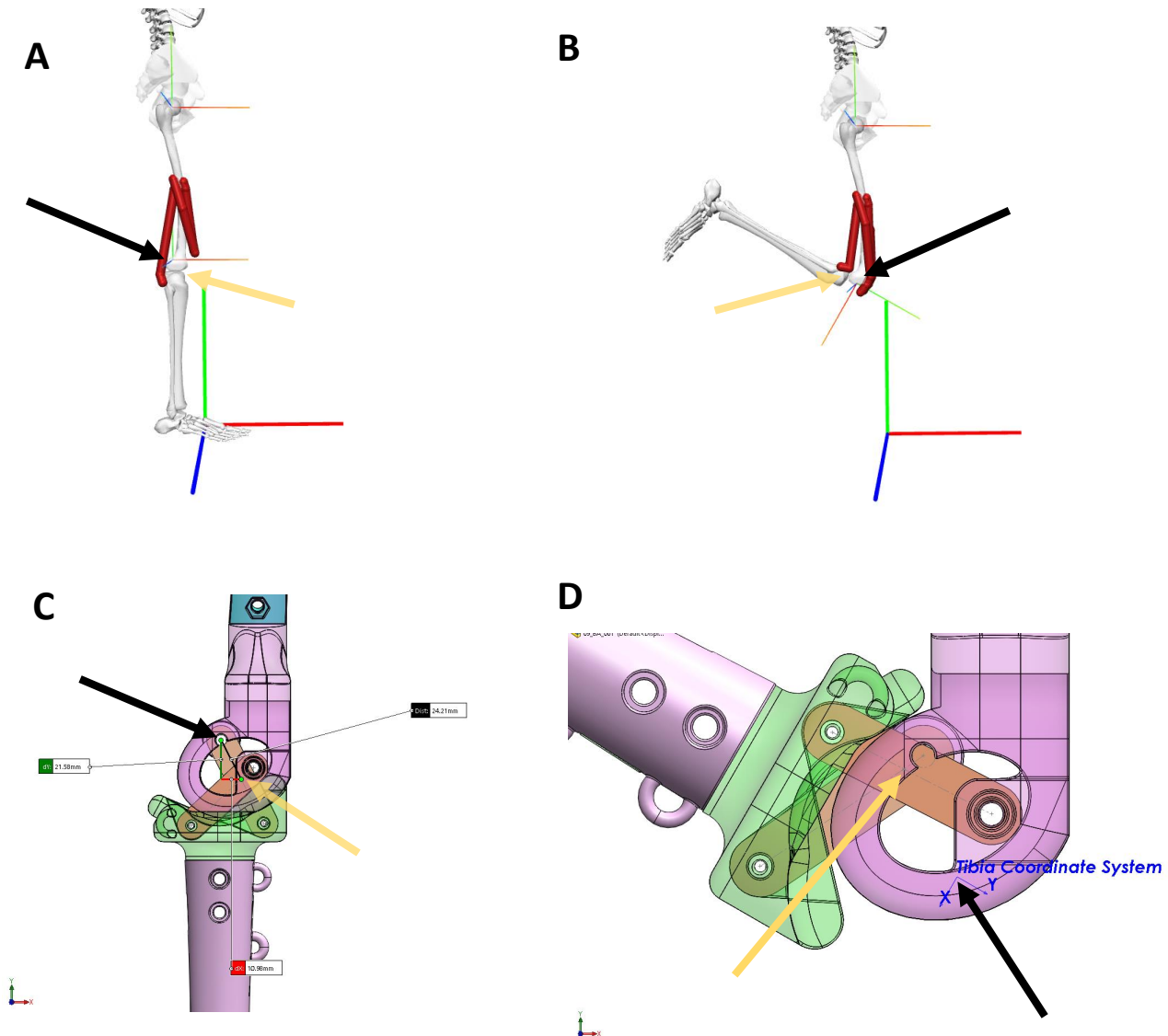


**Figure 3.** Reference frames for Gait2392 in (A) home position and (B) flexed ( $\theta = -120^\circ$ ). Frames for biomimetic robot knee in (C) home position and (D) flexed ( $\theta = -120^\circ$ ). Coordinate directions are:  $\hat{x}$  in red,  $\hat{y}$  in green, and  $\hat{z}$  in blue. Spatial frame is  $s$  and body frame is  $b$ . For (A) and (B): black arrows point to the tibia reference frame as defined by OpenSim, yellow arrows point to the actual ICR (the tibial-femoral contact point), the large axes are general space frames, and the small axes represent body frames for the hip  $h$  and knee  $k$ . For (C) and (D): black arrows point to the tibia reference frame as arbitrarily defined by us ( $\vec{p}_k$  is at  $\theta_3$  (see (Steele et al., 2017) for details) when knee angle  $\theta_k = 0$  and follows a similar path to the Gait2392 model), yellow arrows point to the actual ICR (intersection point of the two links).

et al., 2013; Millard et al., 2013; Thelen, 2003). Reference human values were obtained using the Gait2392 model in the biomechanical modeling software OpenSim (Delp et al., 1990; Seth et al., 2011, 2018). Gait2392 is the anatomical human biomechanical model used for comparison 5. Moment arm  $r_\theta$  is calculated by these sources using the following formula.

$$r_\theta = \frac{dl}{d\theta} \quad (2)$$

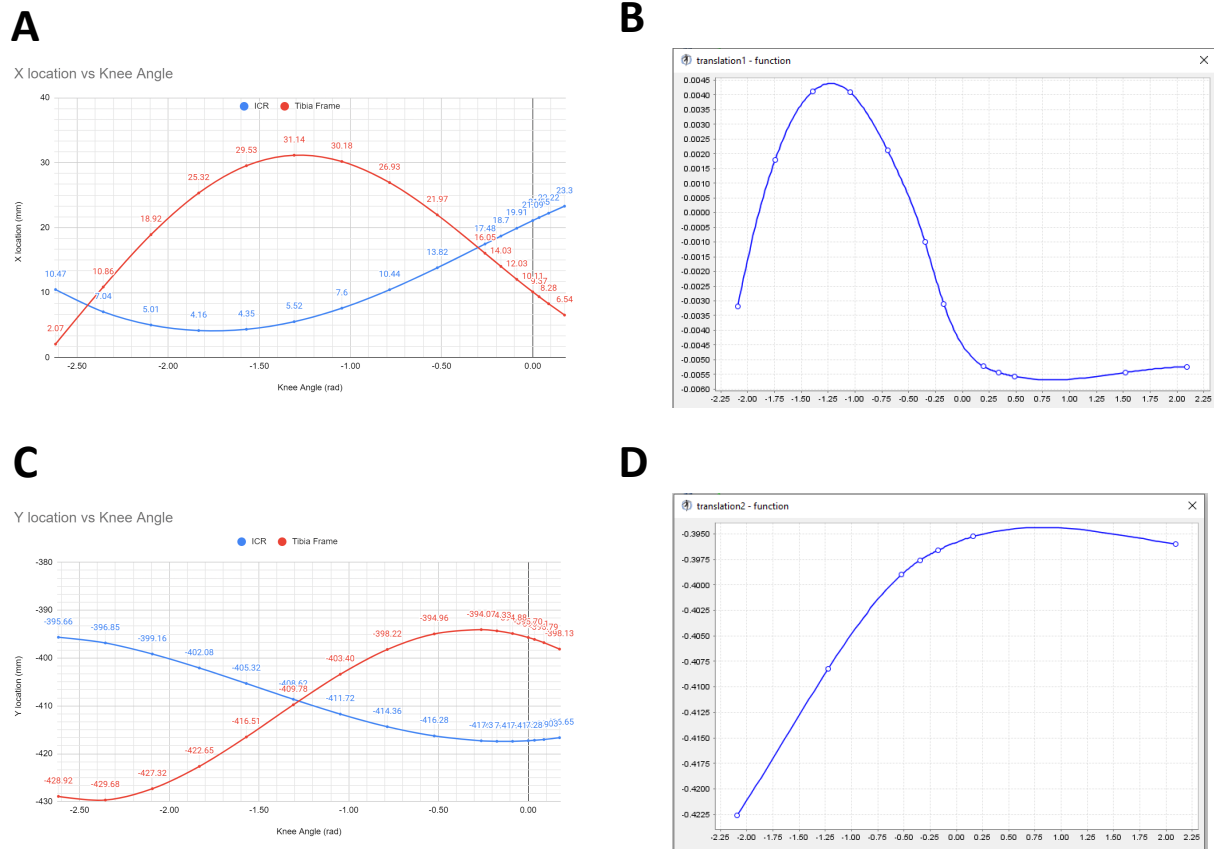


**Figure 4.** Comparison of joint X and Y positions (with respect to femur frame origin) as a function of knee angle. **(A):** X axis location (in millimeters) for tibial frame (red) and ICR (blue) for the biomimetic knee as a function of knee angle (in radians). **(B):** X axis location (in meters) for tibial frame as a function of knee angle (radians). **(C):** Y axis location (in millimeters) for tibial frame (red) and ICR (blue) for the biomimetic knee as a function of knee angle (in radians). **(D):** Y axis location (in meters) for tibial frame as a function of knee angle (radians).

where  $dl$  is the change in muscle length and  $d\theta$  is the change in joint angle. We opted out of using this method. Instead, we used the method developed by Young and colleagues (Young et al., 2019). The moment arm length for moments that produce torque about the  $\hat{z}$  axis is  $r_{\hat{k}}$ .

$$r_{\hat{k}} = p_{proj,i} \cdot \frac{\vec{p}_f \times \hat{k}}{\|\vec{p}_f \times \hat{k}\|} \quad (3)$$

$p_{proj,i}$  is the free muscle segment projected onto the plane of interest defined by the joint axis.  $\vec{p}_f$  is the projected muscle segment vector.

## 2.3 Data Collection: Equipment and Procedures

We built a test stand to take isometric knee torque measurements at different knee angles over its RoM. The test stand frame is made predominantly out of 80/20 components. The knee joint is allowed to rotate while the femur is fixed to the frame. A force sensor has one end connected to the tibia and the other is connected to a swing arm. The swing arm is tied to the winch with 3/16 inch Kevlar rope from Quality™





**Figure 5.** View of the human biomechanical model Gait2392 used for comparison. In this test we looked at the uniarticular muscles that attach to the femur and cross the knee, shown as red muscle actuators in the picture.

170 Nylon Rope 6. This rope has a Kevlar core with a polyester jacket and is rated to have a break strength of  
171 1150 lbs.

172 Force data was collected using one of two different sensors. The first was a MODERN STEP 300 kg digital  
173 crane scale. The second force sensor is a CALT DYLY-103 100 kg S shaped load cell. The was load cell was  
174 used in conjunction with a HX711 Load Cell Amplifier. Pressure data came from a Freescale MPX5700  
175 GP 5 V pressure sensor. Building air supply pressure was controlled with two pressure regulators in series.

176 The first is a Parker model 20R113GC 0-120 *psi* pressure regulator. The second is a Husky 3/8 *in.* High  
 177 Performance Air Regulator HDA72200. A Festo VTUG-10-MRCR-S1T-26V20-T516LA-UL-T532S-8K  
 178 valve manifold VTUG-G was used to deliver air from the pressure regulator to the actuator. This manifold  
 179 is comprised of eight two-in-one bidirectional normally closed Festo VUVG-S10-T32C-AZT-M5-1T1L  
 180 valves.

181 Pressure and load cell amplifier data are sent to Matlab via an Arduino Uno style Sparkfun BlackBoard  
 182 C microcontroller. The computers that used Matlab were running Windows 10 and Windows 11. During  
 183 phases when the Arduino was collecting force and pressure data to send to Matlab, the Arduino would also  
 184 trigger (via Matlab) an onsemi 2N4401 NPN transistor to make valve manifold opened or close the valve.  
 185 For other data collection the valve was manually opened and closed 7.

186 Length measurements were done using a FANUC tape measure. When measuring the knee extensor  
 187 length, at times this was done by using a flexible piece of string to determine the axial length, then  
 188 measuring that string with the tape measure. Other times we were able to measure the extensor length using  
 189 iBayam flexible tape measures.

190 Angle measurements were taken with either a Medigauge digital electronic goniometer or with  
 191 MALENOO analog goniometers of 6, 8, or 12 inch lengths. The angle of the knee joint and the angle of  
 192 the force sensor to the moment arm were the measurements of interest to us. The latter angle allows us to  
 193 calculate torque as the force sensor was not always perpendicular with the moment arm.

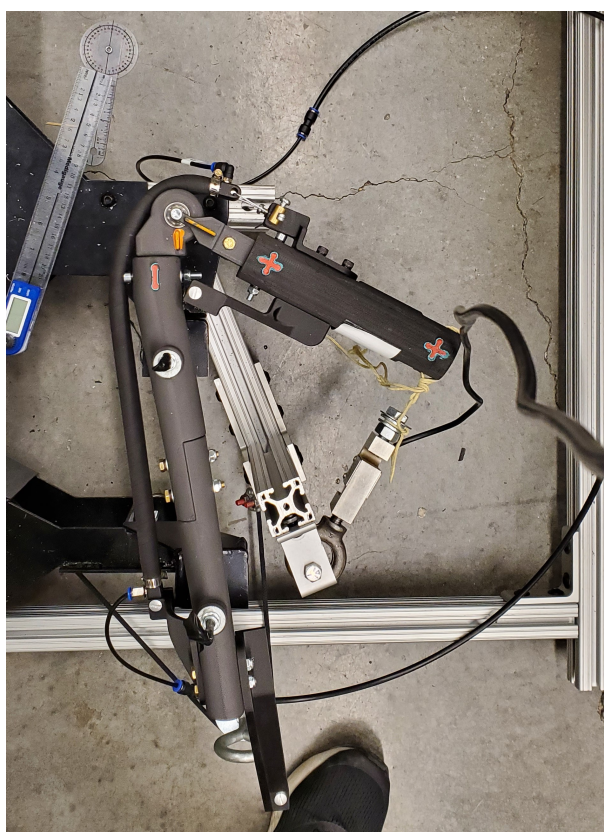


**Figure 6.** Robot leg in test jig. Setup shows the pinned knee configured for a test of the extensor BPA. The knee is positioned at  $\theta_k = -120^\circ$  flexion. The S shaped load cell attaches the tibia to the swing arm and is nearly perpendicular to the tibia in this configuration. Also note the compressed shape of the BPA during this high degree of flexion.

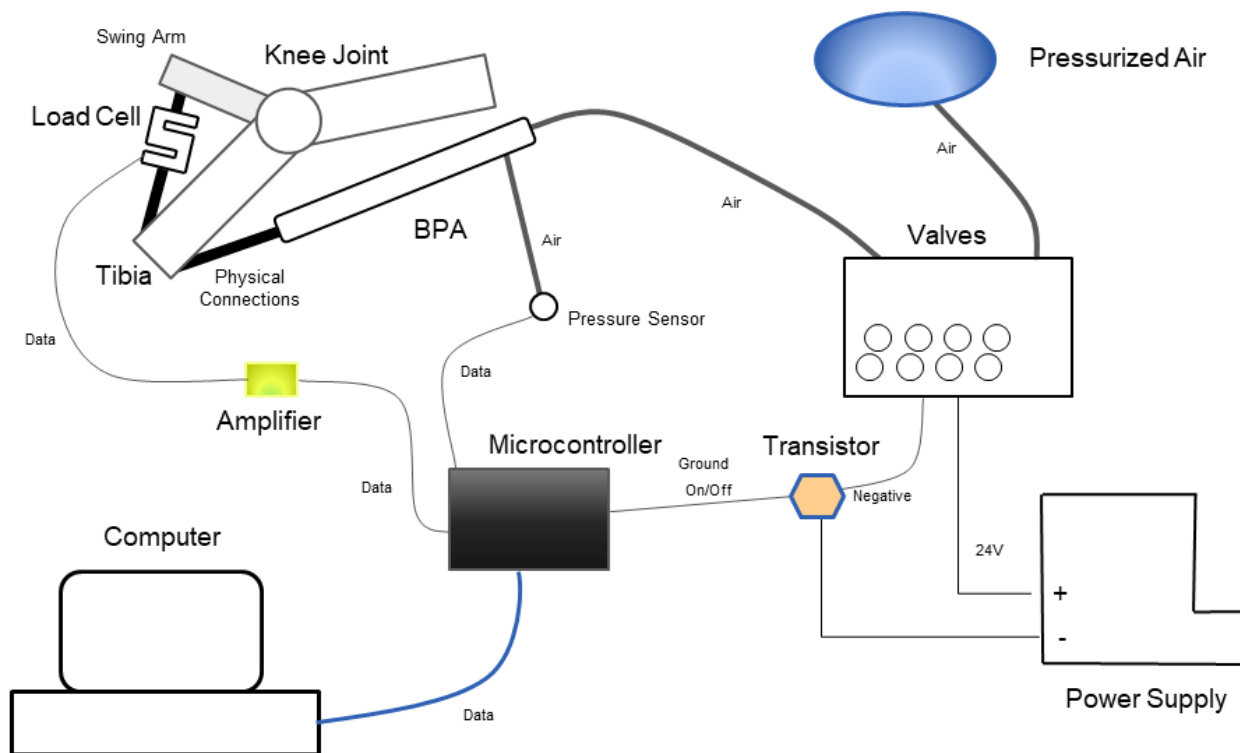


**Figure 7.** Data collection setup

## 194 2.4 Actuator Force Calculation

195 Human muscle-actuator force is calculated using the Hill muscle model. Specifically, we relied on the  
 196 equations as described by Millard (Millard et al., 2013) and used in OpenSim model Gait 2392. The  
 197 specifics equation and values are detailed in previous work by Bolen and Morrow (Bolen and Hunt, 2019;  
 198 Morrow et al., 2020).

199 BPA actuator force in our previous work has been calculated from a length-tension-pressure relationship  
 200 derived by Hunt (Hunt et al., 2017). For a given robot configuration and BPA pressure  $P$  (in kPa), the  
 201 scalar force  $F$  (in Newtons) for each of the artificial muscles can be determined by solving the equation:

$$P = 254 \text{ kPa} + 1.23 \frac{\text{kPa}}{\text{N}} \cdot F + 15.6 \text{ kPa} \cdot S + 192 \text{ kPa} \cdot \tan \left( 2.03 \left( \frac{\epsilon}{-0.331 \times 10^{-3} \frac{1}{\text{N}} \cdot F + \epsilon_{max}} - 0.46 \right) \right) \quad (4)$$

202  $\epsilon$  is the amount of contraction, and  $\epsilon_{max}$  is the maximum amount of contraction in a BPA without external  
 203 load that is inflated to 620 kPa.  $S$  is the hysteresis factor of the artificial muscle in which  $S = 1$  indicates  
 204 the muscle is shortening and with  $S = -1$  it is lengthening. For isometric contraction, set  $S = 0$ . An  
 205 important note for (4) is that the coefficients have been updated with the correct values. We used this  
 206 corrected version of the equation to create a lookup table for actuator force for a given amount of pressure  
 207 and relative strain  $\epsilon^*$ , defined as

$$\epsilon^* = \frac{\epsilon}{\epsilon_{max}} \quad (5)$$

208 With this lookup table created it is possible to use a curve fit to develop an equation for force as a function  
 209 of pressure and relative strain. However, we note here two problems with the BPA characterization in  
 210 (Hunt et al., 2017). The first is that this testing was done with a maximum of 111.2 N applied load, which  
 211 is only about 20% of the maximum isometric force the Festo BPA is rated for at maximum pressure and  
 212 no contraction. Secondly, we observed that maximum force in the BPAs decrease as the resting length  
 213 decreases. Therefore, we created a test jig apparatus to test isometric force for various resting lengths of  
 214 10 mm Festo BPAs at different pressures.

215 Each BPA resting length,  $l_{rest}$ , is measured as the distance between the hose clamps. This is how Festo  
 216 defines  $l_{rest}$ , although in (Hunt et al., 2017) it was measured to also include end cap length. We then  
 217 inflated each BPA to maximum pressure ( $P_{max} = 620$  kPa) and measured  $\epsilon_{max}$ . The BPAs were then  
 218 deflated, placed vertically in the test jig made out of 80/20 pieces and fixed between two crossmembers.  
 219 The force sensor was placed between the upper crossmember and the BPA. For 120 mm, 220 mm, 260 mm,  
 220 281 mm and 281 mm resting lengths, a Loadstar RAS1-01KS-S\*C00 S Shaped load cell was used instead  
 221 of the other force sensors previously mentioned. The distance between the crossmembers was adjusted  
 222 to get different amounts of  $\epsilon^*$ . The BPAs would then be inflated. BPAs with 120 mm, 220 mm, 260 mm,  
 223 281 mm and 281 mm resting lengths had a lot of  $P$  variation, with only 4-5 different values of  $\epsilon^*$  per BPA.  
 224 Conversely, BPAs with resting lengths of 112 mm, 415 mm, 455 mm, 490 mm and 518 mm had many  
 225 different values of  $\epsilon^*$  recorded, but all values were taken at or near  $P_{max}$ . Force and pressure data was  
 226 collected as described in a previous section, above.

### 3 RESULTS

Results from BPA characterization tests are shown first in 8. Fig. 8A and 8B show a force response resembling an arctan curve along the resting length dimension and with a more linear response along the pressure axis. We used a surface fit to find the equation for maximum force as a function of resting length and pressure, i.e.  $F_{max}(l_{rest}, P)$ .

$$F_{max}(l_{rest}, P) = a1 \cdot P \cdot \arctan(a2 \cdot P \cdot (l_{rest} - 0.0075)) \quad (6)$$

$l_{rest}$  was offset by 7.5 mm because modeling showed our end caps would contact at that resting length. Therefore at that length no force could develop since air would flow in one endcap and out the other (assuming perfect alignment). The curve fitting was done using the Nonlinear Least Squares method and a Least Absolute Residual robustness.  $a1 = 0.4848 \text{ N kPa}^{-1}$  (0.4848-0.488 with 95% CI) and  $a2 = 0.03306 \text{ kPa}^{-1} \text{ m}^{-1}$  (0.0325-0.03362 with 95% CI). 6 has an Adjusted  $R^2 = 0.9997$  and an RMSE = 2.749. Substituting  $P_{max} = 620 \text{ kPa}$  into 6 yields the following simplified equation:

$$F_{max}(l_{rest}) = 301.6 \text{ N} \cdot \arctan(20.5 \text{ m}^{-1} \cdot (l_{rest} - 0.0075)) \quad (7)$$

Equation 7 is compared with the data in 8B. It can be seen that  $\lim_{l_{rest} \rightarrow \infty} F_{max} = 473.7 \text{ N}$ . Fig. 8C shows an attempt at a linear fit for  $\epsilon_{max}(l_{rest})$ . There was a large amount of variance in the data, with the linear fit giving an adjusted  $R^2 = 0.4124$  and an RMSE=0.0083, therefore at this time we cannot say with confidence that there is a relationship between maximum strain and resting length.

The next step in BPA characterization we derived an equation for normalized force in the BPA, or  $F^* = F/F_{max}$ . In previous work we have already used relative strain  $\epsilon^* = \epsilon/\epsilon_{max}$ , and here we will also introduce relative pressure  $P^* = P/P_{max}$ . Then we can show that  $F^*(\epsilon^*, P^*)$  9. By visualizing the lookup tables discussed above, and the Festo Corporation data sheet, we can see that there appears to be an exponential relationship between  $\epsilon^*$  and  $F$ , and a linear relationship between  $P^*$  and  $F$ . A polynomial surface fit also shows an interaction between the linear  $P^*$  and exponential  $\epsilon^*$  terms. Therefore we fit a surface to the original data using an equation of the form

$$F^*(\epsilon^*, P^*) = b0 + b2 \cdot \exp(-b1 \cdot \epsilon^*) + b4 \cdot P^* \exp(-b3 \cdot (\epsilon^*)^2) + b5 \cdot P^* \quad (8)$$

With all the additional data collected on 10 mm BPAs with resting lengths given in 8, we then normalized the force data collected by dividing a BPA's force results by the maximum amount of force that BPA could produce at 620 kPa. This reduced much of the variance in the data, as shown in Fig. 9, which qualitatively pointed towards using a surface fit as the right approach for  $F^*$ . Using  $\epsilon^*$  and  $P^*$ , it was possible to reduce the amount of coefficients in Eq. 8 from six to only two. The equation for normalized force is

$$F^*(\epsilon^*, P^*) = -1 + \exp(-b1 \cdot \epsilon^*) + P^* \exp(-b2 \cdot (\epsilon^*)^2) \quad (9)$$

with  $b1 = 1.7$  (1.692-1.708 with 95% CI) and  $b2 = 0.2$  (0.1968-0.2029 with 95% CI). This surface fit was done using Nonlinear Least Squares method and Least Absolute Residuals robustness. Additional data from separate tests using the 120 mm, 220 mm, 260 mm, 281 mm and 281 mm resting lengths were used for validation. Eq. 9 has an Adjusted  $R^2 = 0.9998$ , SSE = 0.007833, and an RMSE = 0.0057. Validation SSE



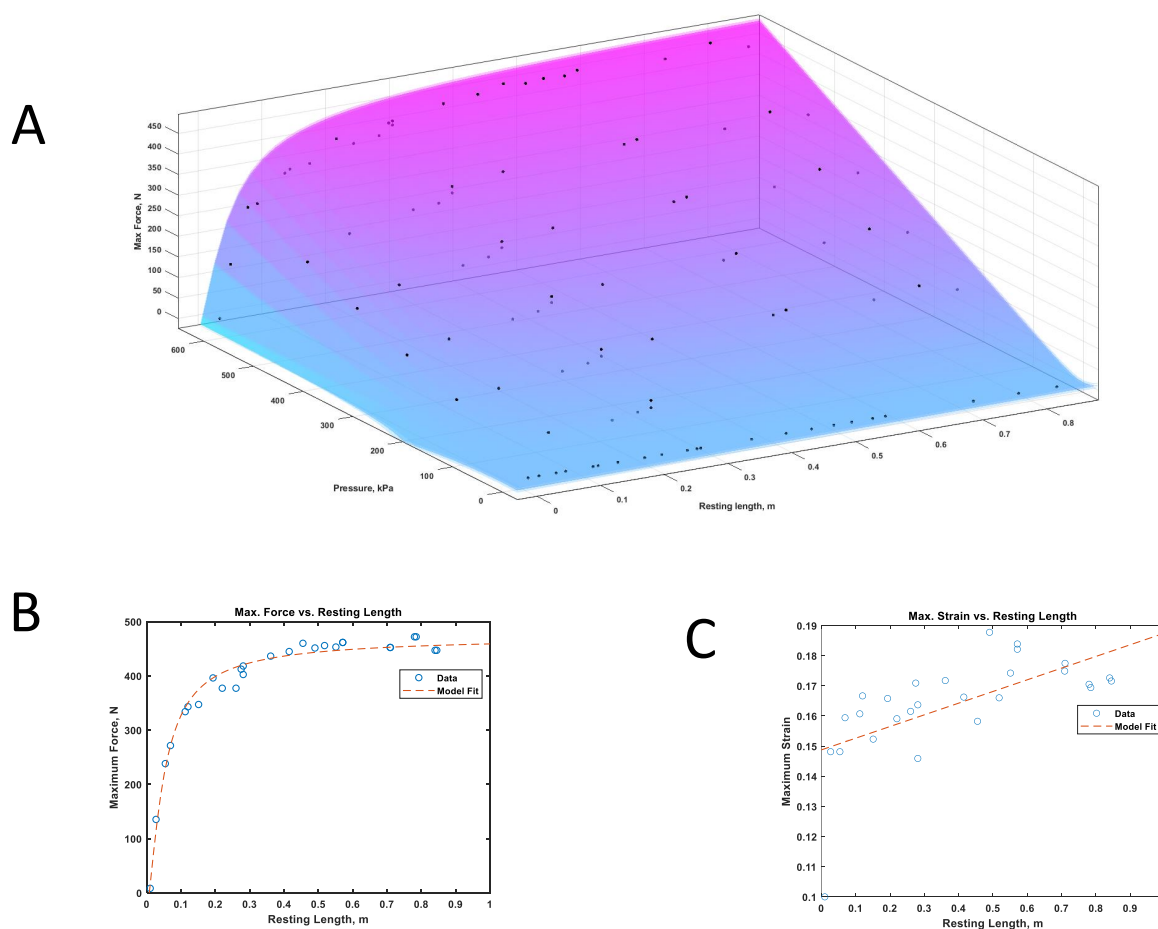


**Figure 8.** Results for finding the relationship between  $l_{rest}$  and  $F_{max}$ ,  $\epsilon_{max}$ . **(A)** Surface fit for  $F_{max}(l_{rest}, P)$ . **(B)**  $F_{max}$  versus  $l_{rest}$  at  $P_{max} = 620$  kPa. **(C)**  $\epsilon_{max}$  versus  $l_{rest}$  at  $P_{max} = 620$  kPa. No conclusive relationship between  $\epsilon_{max}$  and  $l_{rest}$  could be deduced from this experiment.

257 = 0.482595 and RMSE = 0.044292. Combining Eq. 9 and Eq. 7 will now allow researchers to determine  
 258 the force  $F$  in a BPA given  $l_{rest}$ ,  $P$ , and  $\epsilon^*$ .

259 10 mm pinned knee flexor results. Simplest case that doesn't require the BPA to bend.

260 10 mm pinned knee extensor results. How previous optimization works with these results.

261 Opensim comparison.

262 Full size knee assembly results.

263 10 mm 2-DoF knee results.

264 10 mm pinned knee extensor of same resting length but with tendon, without tendon, and changed muscle  
 265 routing.

266 Graphs showing torques for flexor muscle lengths with either biomimetic knee. 10

267 Graphs showing torques for extensor muscle lengths with either biomimetic or pinned knee.



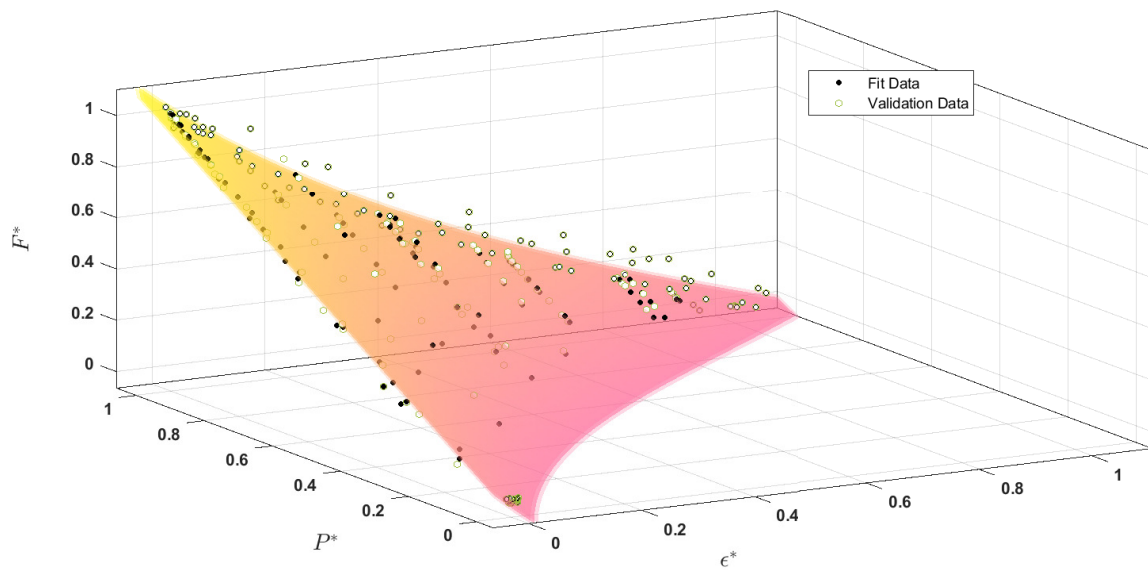


**Figure 9.** Surface fit for  $F^*(\epsilon^*, P^*)$ . Fit Data is solid black circles, validation data is the green circles.

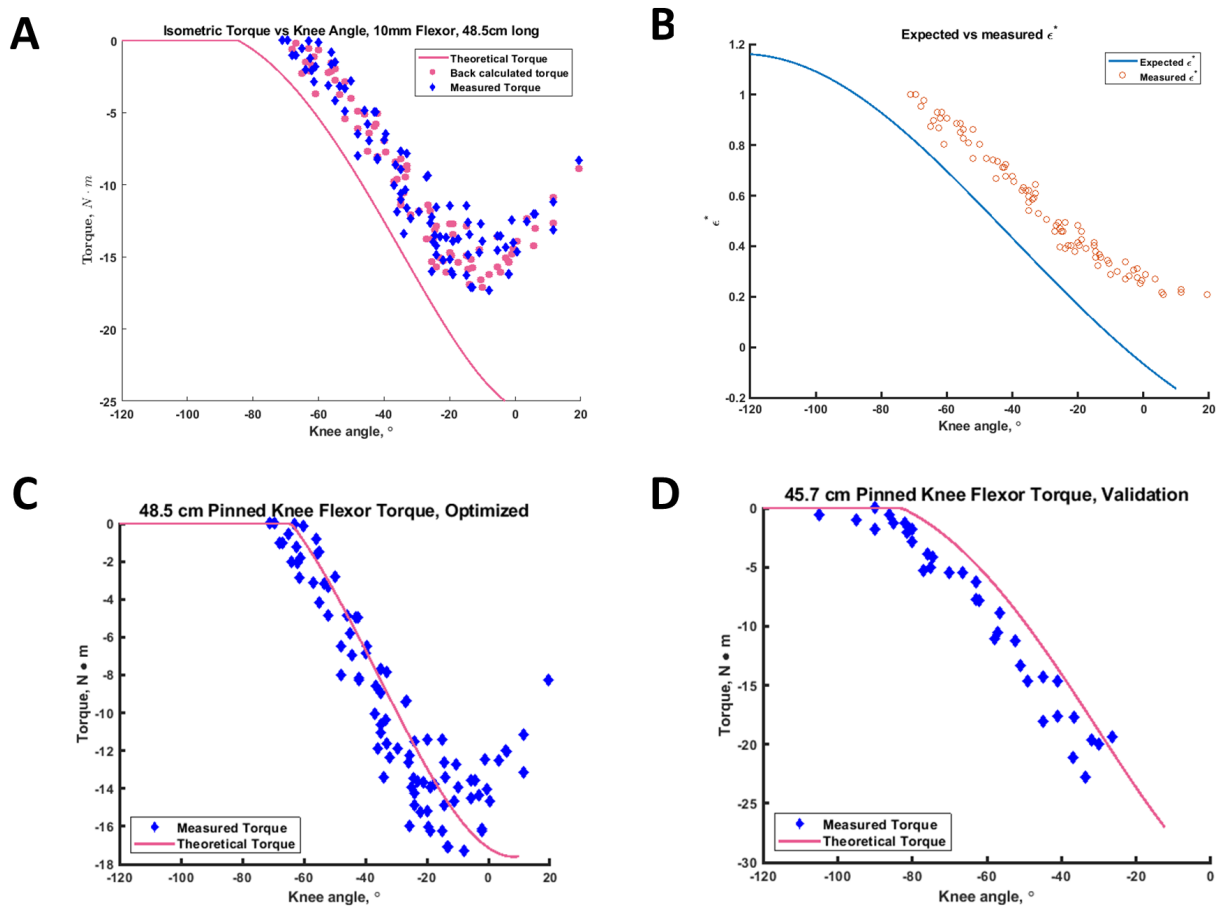


**Figure 10.** Results for the pinned knee using flexor BPAs of length (A) 48.5 cm and (B) 45.5 cm.

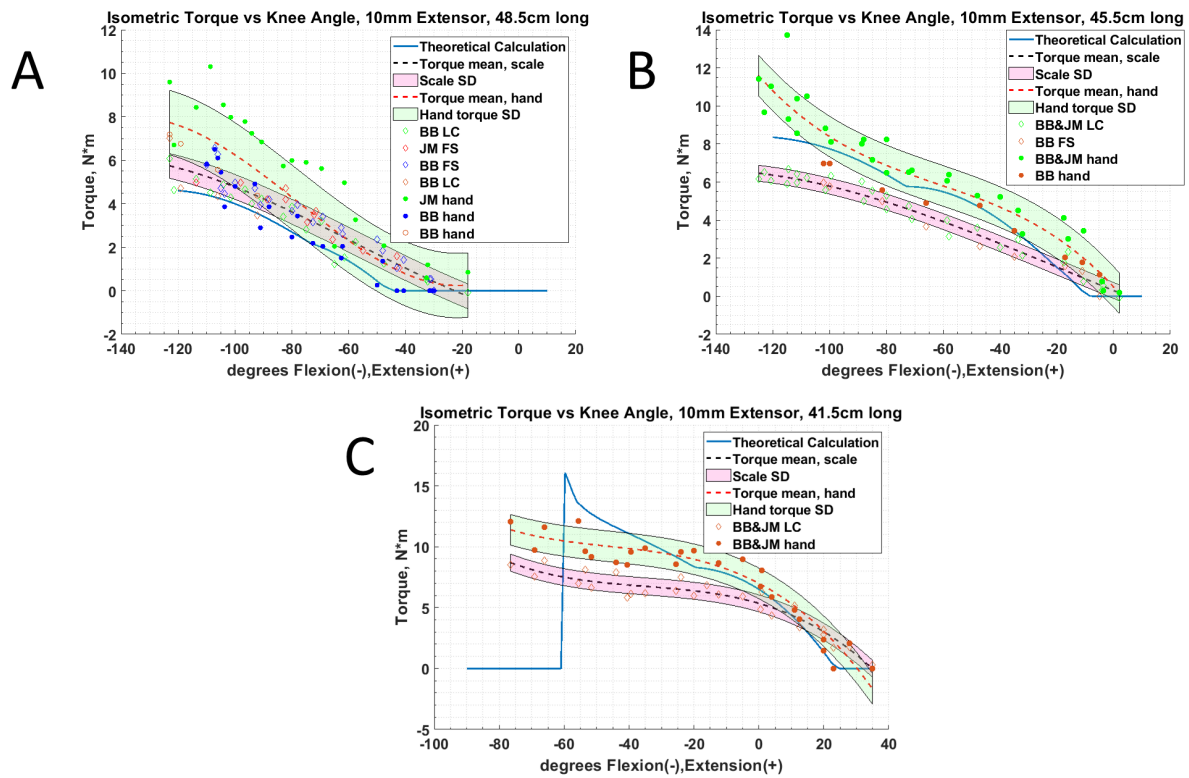
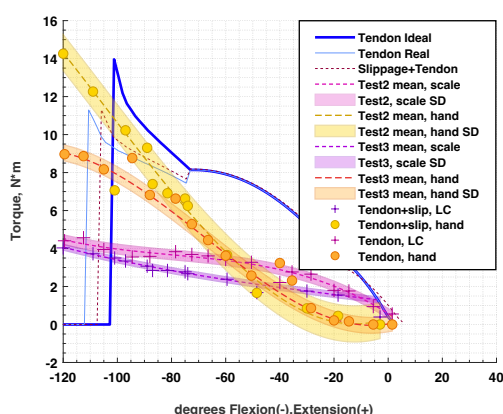
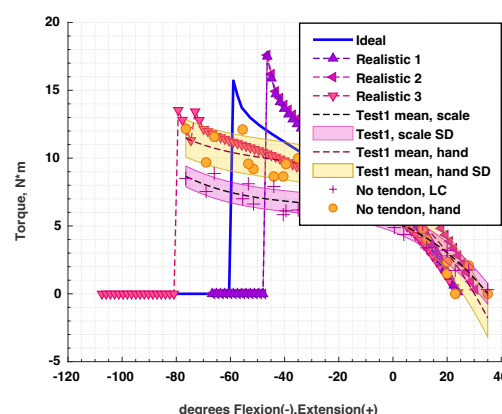


**Figure 11.** Pinned knee isometric torque with the extensor BPA for lengths, (a) 48.5 cm, (A) 45.5 cm, and (c) 41.5 cm

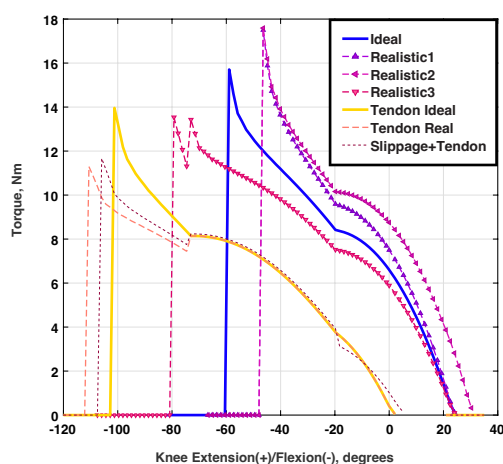
Z axis Torque, 10mm Extensor, 41.5cm long, no tendon



Z axis Torque, 10mm Extensor, 41.5cm long, 22 mm tendon



BPA Z Torque, Length = 415 m



BPA X Torque, Length = 415 mm

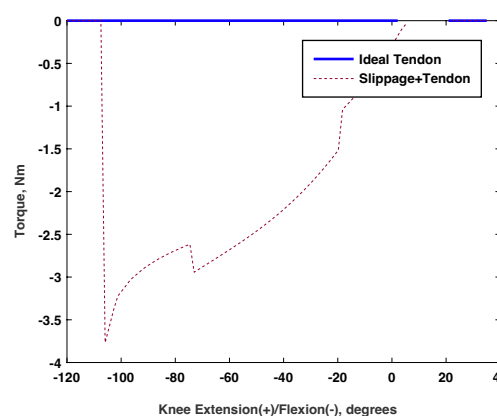


**Figure 12.** Isometric knee torque for a 10 mm diameter extensor actuator with a 41.5 cm long resting length. **(A)** Expected and measured results are shown when using a 22 mm artificial tendon. **(B)** No tendon, measured results vs. expected for ideal scenario and others. **(C)** Expected results are shown for a 42 cm resting length BPA. Normal case (ideal), resting length minus 8 mm (Realistic 1), fitting length minus 8 mm (Realistic 2), resting length plus 8 mm (Realistic 3), expected results using a 22 mm long tendon (Tendon Ideal), expected results compensating for insertion bracket being slightly bent and the distal part of the BPA being stretched and compressed (Tendon Real), and expected values after noticing that the BPA would take a routing path different than we thought (Slippage+Tendon). **D** shows the change in X axis Torque between expected values between specified muscle path and the BPA with +20 z displacement due to it not contacting the screw connecting the knee to the femur.

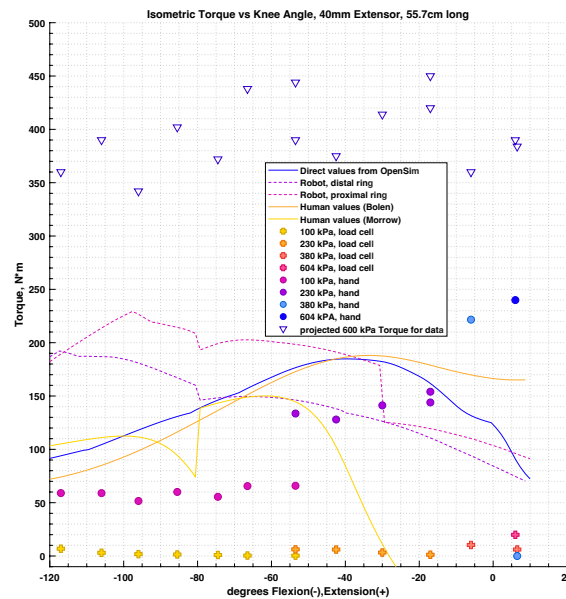


**Figure 13.** Comparison of isometric torque for theoretical BPA values with the humanoid knee, human muscle calculations using our method, and human muscle values as provided by OpenSim. Configurations listed are for (A) flexor and (B) extensor muscles. Note the major discrepancies between the our human value and OpenSim's, which calls into question the accuracy of our calculations.



**Figure 14.** Results vs. expected using 10 mm BPAs on the biomimetic knee in (A) flexor and (B) extensor configurations.



**Figure 15.** Results vs. expected values on the biomimetic knee with a 40 mm BPA in the extensor configurations.

## 4 DISCUSSION

268 There certainly are many factors that affect the isometric torque results.

269 Simplifying the model and testing it allowed us to see how we were deficient in our previous analysis.  
270 The isometric system is not rigid. It adds springiness, not

271 Curving BPA during high angles of knee flexion show the BPA being stretched and compressed. It is  
272 known that the axial stress in a pressure vessel is

$$\sigma_z = \frac{F}{A} = \frac{Pd^2}{(d + 2t)^2 - d^2} \quad (10)$$

273 Where  $\sigma_z$  is the axial stress,  $F$  is Force,  $A$  is area,  $P$  is the internal pressure,  $t$  is the wall thickness, and  $d$   
274 is the mean diameter ( $O.D. - t$ ). In thin wall pressure vessels 10 can be reduced to

$$\sigma_z = \frac{Pd}{4t} \quad (11)$$

## RESOURCE IDENTIFICATION INITIATIVE

## CONFLICT OF INTEREST STATEMENT

275 The authors declare that the research was conducted in the absence of any commercial or financial  
276 relationships that could be construed as a potential conflict of interest.

## AUTHOR CONTRIBUTIONS

277 BB, CM, and AH contributed to conception and design of the study. BB and CM wrote the code to calculate  
278 theoretical human and robot isometric torques. Figures were created by BB and AV. BB, LB, and AV wrote  
279 code for data collection and analysis. BB collected the data and performed the statistical analysis. BB  
280 organized the database. BB wrote the first draft of the manuscript. BB, LB, and AH wrote sections of the  
281 manuscript. All authors contributed to manuscript revision, read, and approved the submitted version.

## FUNDING

282 Research for this article was funded by the Department of Mechanical and Materials Engineering at  
283 Portland State University, the National Science Foundation (NSF) grant for NeuroNex: Communication,  
284 Coordination, and Control in Systems (C3NS) 2015317 and NSF grant 1943483.

## ACKNOWLEDGMENTS

285 The authors would like to acknowledge the contribution of Alex Steele, who designed the initial biomimetic  
286 4-bar knee linkage we used for the test. He gave us solid models, built a 3D prototype, and let us break said  
287 prototype. His prompt and thoughtful responses to our questions about the previous design was very much  
288 appreciated. The authors would also like to thank Jasmine Bradley for her help reworking the figures in the  
289 results section. As a visual designer, her contributions improved the aesthetic quality of the images. She  
290 also helped us choose colors that ensured data accessibility for people with color blindness.

## SUPPLEMENTAL DATA

291 Supplemental Data includes figures for the test setup.

## DATA AVAILABILITY STATEMENT

292 The data sets are available from the authors upon request.

## REFERENCES

- 293 Asano, Y., Okada, K., and Inaba, M. (2019). enMusculoskeletal design, control, and application of human  
294 mimetic humanoid Kenshiro. *Bioinspiration & Biomimetics* 14, 036011. doi:10.1088/1748-3190/ab03fc  
295 Bolen, B. P. and Hunt, A. J. (2019). enDetermination of Artificial Muscle Placement for Biomimetic  
296 Humanoid Robot Legs. In *Biomimetic and Biohybrid Systems*, eds. U. Martinez-Hernandez, V. Vouloutsi,  
297 A. Mura, M. Mangan, M. Asada, T. J. Prescott, and P. F. Verschure (Cham: Springer International  
298 Publishing), vol. 11556. 15–26. doi:10.1007/978-3-030-24741-6\_2  
299 [Dataset] Corporation, F. (2022). Festo Fluidic Muscle DMSP



- Delp, S., Loan, J., Hoy, M., Zajac, F., Topp, E., and Rosen, J. (1990). An interactive graphics-based model of the lower extremity to study orthopaedic surgical procedures. *IEEE Transactions on Biomedical Engineering* 37, 757–767. doi:10.1109/10.102791
- Hoy, M., Zajac, F., and Gordon, M. (1990). A musculoskeletal model of the human lower extremity: the effect of muscle, tendon, and moment arm on the moment-angle relationship of musculotendon actuators at the hip, knee, and ankle. *Journal of Biomechanics* 23, 157–169
- Hunt, A., Graber-Tilton, A., and Quinn, R. (2017). Modeling length effects of braided pneumatic actuators. In *IDETC/CIE 2017* (Cleveland, OH: ASME)
- Millard, M., Uchida, T., Seth, A., and Delp, S. L. (2013). Flexing Computational Muscle: Modeling and Simulation of Musculotendon Dynamics. *Journal of Biomechanical Engineering* 135, 021005. doi:10.1115/1.4023390
- Morrow, C., Bolen, B., and Hunt, A. (2020). Optimization of Artificial Muscle Placements for a Humanoid Bipedal Robot. In *Biomimetic and Biohybrid Systems*
- Seth, A., Hicks, J. L., Uchida, T. K., Habib, A., Dembia, C. L., Dunne, J. J., et al. (2018). OpenSim: Simulating musculoskeletal dynamics and neuromuscular control to study human and animal movement. *PLOS Computational Biology* 14, e1006223. doi:10.1371/journal.pcbi.1006223
- [Dataset] Seth, A., Sherman, M., Reinbolt, J. A., and Delp, S. L. (2011). OpenSim: a musculoskeletal modeling and simulation framework for in silico investigations and exchange.
- Sherman, M. A., Seth, A., and Delp, S. L. (2013). What is a Moment Arm? Calculating Muscle Effectiveness in Biomechanical Models Using Generalized Coordinates. In *Volume 7B: 9th International Conference on Multibody Systems, Nonlinear Dynamics, and Control* (Portland, Oregon, USA: American Society of Mechanical Engineers), V07BT10A052. doi:10.1115/DETC2013-13633
- Shin, H., Ikemoto, S., and Hosoda, K. (2018). Constructive understanding and reproduction of functions of gluteus medius by using a musculoskeletal walking robot. *Advanced Robotics* 32, 202–214. doi:10.1080/01691864.2018.1434015. Publisher: Taylor & Francis
- Steele, A., Hunt, A., and Etoundi, A. (2018). Biomimetic Knee Design to Improve Joint Torque and Life for Bipedal Robotics (Bristol, UK)
- Steele, A. G., Hunt, A., and Etoundi, A. C. (2017). Development of a Bio-inspired Knee Joint Mechanism for a Bipedal Robot. In *Biomimetic and Biohybrid Systems* (Springer, Cham), Lecture Notes in Computer Science, 418–427. doi:10.1007/978-3-319-63537-8\_35
- Thelen, D. G. (2003). Adjustment of Muscle Mechanics Model Parameters to Simulate Dynamic Contractions in Older Adults. *Journal of Biomechanical Engineering* 125, 70–77. doi:10.1115/1.1531112
- Yamaguchi, G. T. and Zajac, F. E. (1989). A planar model of the knee joint to characterize the knee extensor mechanism. *Journal of Biomechanics* 22, 1–10. doi:10.1016/0021-9290(89)90179-6
- Young, F., Rode, C., Hunt, A., and Quinn, R. (2019). Analyzing Moment Arm Profiles in a Full-Muscle Rat Hindlimb Model. *Biomimetics* 4, 10. doi:10.3390/biomimetics4010010

## FIGURES

## TABLES

**Table 1.** Muscle origin and insertion locations for different models. Origin is in femur reference frame, insertion is in the tibia reference frame.

Muscle	Origin/Insertion	Model	X (m)	Y (m)	Z (m)
Flexor	origin	Pinned knee	-0.075	0.100	0.0328
Flexor	insertion	Pinned knee	-0.05011	-0.045	0.0326
Extensor	origin	Pinned knee	0.030	-0.050	0
Extensor	insertion	Pinned knee	0.0425	-0.076	0
Bifemsh	origin	Gait2392	0.005	-0.211	0.023
Bifemsh	insertion	Gait2392	-0.03	-0.036	0.029
Vastus int.	origin	Gait2392	0.029	-0.192	0.031
Vastus int.	insertion	Gait2392	moving	moving	0.0018
Flexor, 10 mm	origin	Biomimetic knee	-0.050	-0.045	0.0328
Flexor, 10 mm	insertion	Biomimetic knee	-0.0279	-0.046	0.0328
Extensor, 10 mm	origin	Biomimetic knee	0.040	0.035	0
Extensor, 10 mm	insertion	Biomimetic knee	0.021	-0.072	0
Flexor, 40 mm	origin	Biomimetic knee	-0.050	-0.045	0.0328
Flexor, 40 mm	insertion	Biomimetic knee	-0.0279	-0.046	0.0328
Extensor, 40 mm	origin	Biomimetic knee	0.040	0.035	0
Extensor, 40 mm	insertion	Biomimetic knee	0.022	-0.072	0